

Discovering Ferroelectric Plastic (Ionic) Crystals in the Cambridge Structural Database: Database Mining and Computational Assessment

Elin Dypvik Sødahl,^{1,*} Seyedmojtaba Seyedraoufi,¹ Carl Henrik Görbitz,² and Kristian Berland^{1,†}

¹*Department of Mechanical Engineering and Technology Management, Norwegian University of Life Sciences, 1432 Ås, Norway.*

²*Department of Chemistry, University of Oslo, 0371 Oslo, Norway.*

(Dated: June 14, 2023)

Hybrid or organic plastic crystals have the potential as lead-free alternatives to conventional inorganic ferroelectrics. These materials are gaining attention for their multiaxial ferroelectricity, above-room-temperature Curie temperatures, and low-temperature synthesis. Here, we report a screening study of the Cambridge Structural Database (CSD) resulting in 55 new candidate plastic and plastic ionic ferroelectric molecular crystals, along with 16 previously reported ferroelectrics. With over 1.2 million entries in the CSD, the screening procedure involved many steps, including considerations of molecular geometry and size, space group, and hydrogen bonding pattern. The spontaneous polarization and electronic band gaps were predicted using density functional theory. 21 of the candidate ferroelectrics have a polarization greater than $10 \mu\text{C}/\text{cm}^2$, out of which nine are reported at room temperature.

I. INTRODUCTION

Plastic crystals are molecular crystals characterized by the existence of an orientationally disordered mesophase. In the mesophase, the material becomes ductile, i.e., “plastic”, due to both reduced intermolecular bonding and increased symmetry yielding facile slip planes.¹ As a result, plastic crystals can be molded and fused, in stark contrast to most molecular crystals and inorganic ceramics, which tend to be non-flexible and/or brittle.² These materials can be synthesized with low-cost and low-energy methods including co-precipitation, slow evaporation, spin coating, and 3D printing.^{3–8} Plastic crystals can be bonded solely through both van der Waals or hydrogen bonding and such compounds are referred to as the plastic *molecular* crystals, but they can also have an additional ionic component consisting of charged molecular species, which are referred to as plastic *ionic* crystals. Typically, the molecular species of plastic crystals have a quasi-spherical or “globular” shape, which reduces rotational barriers.^{1,3,9–13} In addition to the plastic mesophase, the molecular rotations can imbue the plastic crystals with functional properties such as ferroelectricity.

Ferroelectric plastic crystals can exhibit a rich phase diagram,^{14,15} with multiple competing crystalline phases and the existence of plastic ferroelectric mesophases, as seen in quinuclidinium perrhenate, having partial orientational disorder.³ They can also exhibit multiaxial polarization with as many as 24 equivalent axes,^{13,16–26} and Curie temperatures up to 466 K.^{27,28} For applications such as FeRAM and piezoelectric sensing, a high Curie temperature is essential. Multiaxial

polarization allows the spontaneous polarization to be aligned in a desired direction in polycrystalline systems, and can allow for multi-bit storage in single crystals.²⁹ A key advantage of ferroelectric plastic crystals is the fact that they can exhibit low coercive fields, e.g., for 1-azabicyclo[2.2.1]heptanium perrhenate and quinuclidinium perrhenate values in the 2 – 5 kV/cm range have been reported.^{3,30} Such values are comparable to that of BaTiO₃, a well-known inorganic ferroelectric.³¹ However, their spontaneous polarization tends to be on the lower end, with most reported values falling below $10 \mu\text{C}/\text{cm}^2$.^{3,16,27,32–38}

In 2020, Horiuchi et al. cataloged approximately 80 reported small-molecule ferroelectric crystals.³⁹ This number is in stark contrast to the collection of approximately 1.2 million organic structures in the Cambridge Structural Database (CSD),⁴⁰ which potentially harbors many undiscovered ferroelectric plastic crystals. Screening this database, we recently reported 6 new organic proton-transfer ferroelectric candidates.⁴¹ In this paper, we detail our screening of ferroelectric candidates likely to exhibit plastic properties. For all the identified materials, we used density functional theory (DFT) computations for geometry optimization of the crystal structure and to predict the spontaneous polarization and electronic band gaps. The new compounds identified in this manner are not only of interest in themselves, but can serve as template structures for further crystal engineering, i.e., by substituting molecular species or halides to tune functional properties.

II. METHODS

A. Mining the CSD for Ferroelectric Plastic Crystals

To identify candidate ferroelectric plastic crystals in the CSD, we reduced the number of structures in five

* elin.dypvik.sodahl@nmbu.no

† kristian.berland@nmbu.no

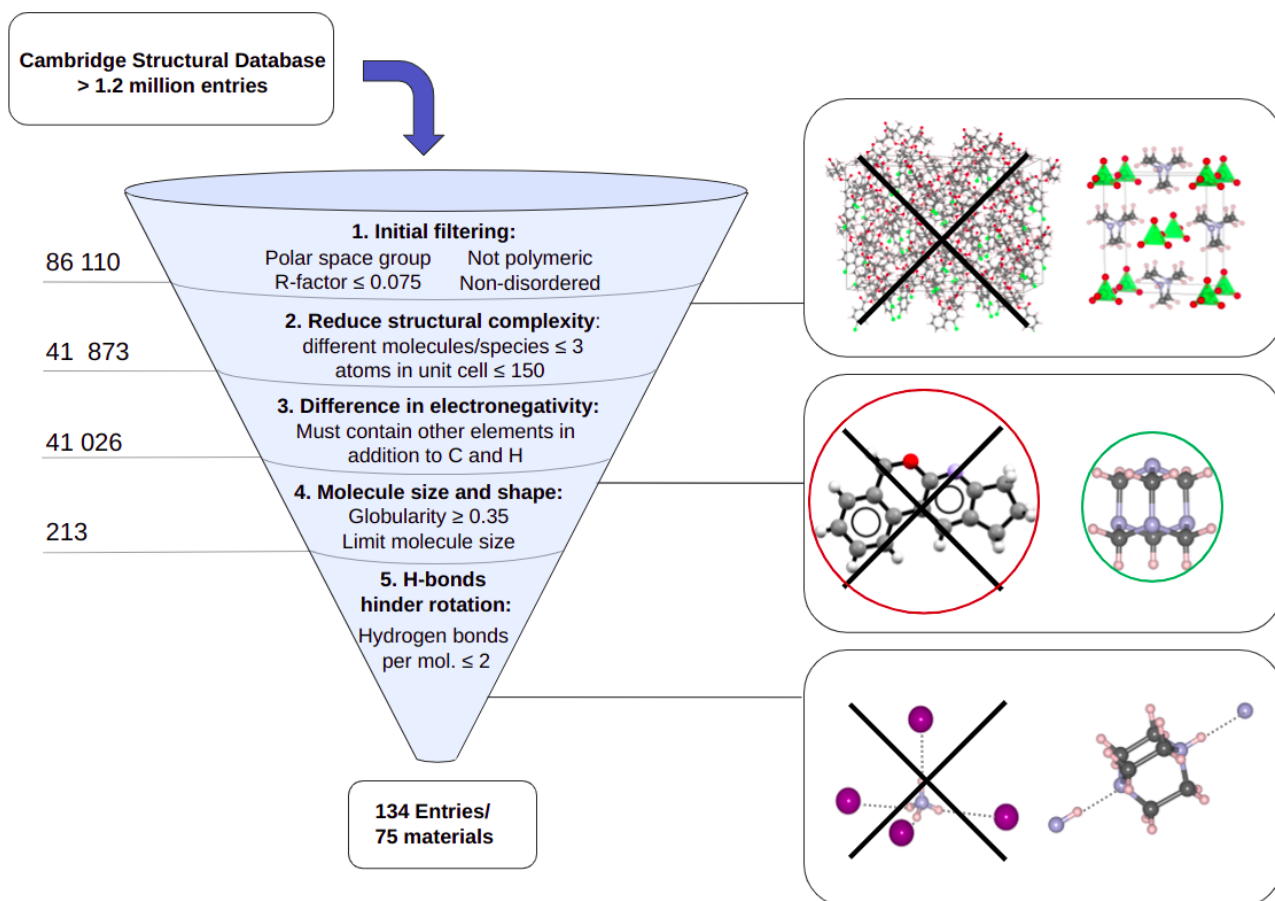


FIG. 1: Overview of the screening procedure to identify ferroelectric plastic crystals in the CSD. The numbers to the left indicate the number of structures remaining after each filtering step.

filtering steps based on the properties of the molecular crystal structure and the constituents molecules, as outlined in Fig. 1. For this procedure, the CSD Python API⁴⁰ and the MOLCRYST⁴² package developed by us, based on the Atomic Simulation Environment⁴³ and the NETWORKX⁴⁴ package were used.

Step 1 excluded non-polar, polymeric, or disordered structures, as well as less accurate structures, i.e., with an R-factor higher than 0.075.

Step 2 excluded structures with unit cells containing more than 150 atoms, removing many complex and large structures. Thus, we avoided time-consuming DFT computations.

Step 3 excluded all materials containing solely C and H. This choice was made as polar covalent bonds or charge transfer between species is needed for high polarization, which requires electronegativity differences.

Step 4 excluded all structures with bulky and/or elongated molecules, as steric hindrance would typically be too large for molecular rotations in a solid phase. Only molecules with 10 or fewer non-hydrogen atoms were retained. Molecular graph theory was used to remove "chainy" molecules, such as all aliphatic

chains longer than four carbon atoms. This is further detailed in Appendix A.

Further, we removed structures that lacked at least one molecule with a globular or semi-globular geometry. As a globularity measure, we used the ratio between the volume of the convex hull and the volume of the smallest bounding sphere of the molecule, excluding hydrogen atoms. With this measure, the C₆₀ fullerene has a globularity of 0.87, while acetic acid has a globularity of 0.10. The smallest allowed globularity was set to 0.35, based on a review of known molecular ferroelectrics. As an example, quinuclidinium perrhenate and iodate are multiaxial ferroelectric plastic ionic crystals with low coercive fields, of respectively 340 and 255 kV/cm, where the quinuclidinium molecule has a globularity of 0.52. In comparison, the non-plastic ferroelectric [Cu-(Hdabco)(H₂O)Cl₃]⁴⁵ has a globularity of 0.24.

Step 5 excluded structures where the globular molecules have more than two hydrogen bonds to avoid 3D hydrogen-bonded networks which would hinder molecular rotations.

After all filters were applied, the pool was reduced

to 75 structures. For each, the spontaneous polarization and electronic band gap were computed using DFT.

While we identified a wide range of candidate materials, the screening criteria have caused some candidates to be omitted. The cap of the number of atoms in the unit cell for instance excluded the ferroelectric metal-free plastic perovskite $[\text{NH}_3 - \text{dabco}]\text{NH}_4\text{I}_3$, as it has 198 atoms in its unit cell. The molecular size limit furthermore excluded some known plastic crystals, such as adamantane derivatives, the C_{60} fullerene,^{46–48} and plastic colloidal crystals.¹⁹ Nonetheless, our target was not to identify all plastic ferroelectrics, but rather identify several of technological interest. Notably, ferroelectric plastic crystals of small molecules would typically have a larger density of dipoles, both originating from individual molecules and inter-molecular charge transfer. Ferroelectric plastic crystals also tend to have ferroelectric phases of high symmetry, resulting in relatively small unit cells.

Finally, this screening procedure does not evaluate if the spontaneous polarization is switchable, as is required for ferroelectrics. The presence of small, globular molecules facilitates a rotational switching mechanism. However, in some of the compounds, the switching path is not clear-cut, and more involved computations or experimental studies have to be performed for a full assessment.

B. Density Functional Theory Calculations

The DFT computations were carried out using the VASP software package^{49–52} with the projector augmented plane wave method (PAW) pseudopotentials.^{53,54} The plane wave cut-off was set to 530 eV for all computations. A Γ -centered Monkhorst-Pack k -point grid with a spacing of $1/15 \text{ \AA}^{-1}$ was used to sample the Brillouin zone. All structures were relaxed until forces fell below 0.01 eV/\AA . The spontaneous polarization was computed using the Berry phase method.^{55,56} Both relaxation and polarization calculations were performed using the vdW-DF-cx functional,⁵⁷ which we found to provide accurate lattice constants in our benchmarking study of exchange-correlation functionals for ferroelectric plastic crystals.⁵⁸

III. RESULTS AND DISCUSSION

Out of the 75 materials identified by screening the CSD, 16 are earlier reported to have ferroelectric properties.^{3,15,16,27,28,32–38,59,60} Four have also been studied for their piezoelectric and/or dielectric properties, but were not reported to be ferroelectric (CSD refcodes: BOXCUO, QIMXER, BOBVIY12, and BOCKEK06).^{61–64,66} Table I lists the available experimental results, as well as the computed spontaneous polarization and electronic band gaps for the earlier re-

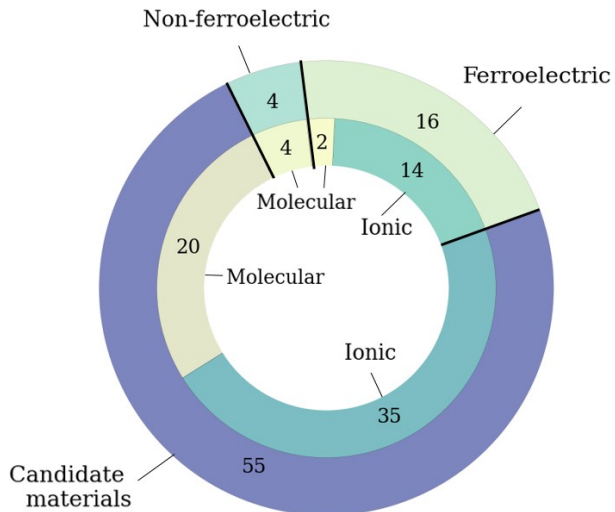


FIG. 2: Overview of the candidate ferroelectrics, reported ferroelectrics, and reported non-ferroelectric materials identified in the screening. The outer circle indicates the number of structures in each of these groups, and the inner circle indicates the number of molecular and ionic molecular crystals.

ported ferroelectrics and non-ferroelectrics, while Table II lists the computed values for the candidate materials. For three of them, the DFT computations did not yield a band gap. This was confirmed using the hybrid functional of Heyd, Scuseria, and Ernzerhof, HSE06,⁶⁷ which does not underestimate band gaps as the vdW-DF-cx functional does due to the lack of non-local exchange.

Fig. 2 shows an overview of the molecular and ionic molecular crystals among the earlier reported and candidate ferroelectrics. Out of the 16 known ferroelectrics, 14 are ionic molecular crystals. For the candidate materials, 20 are molecular, and 35 are ionic molecular crystals.

A selection of the chemical species found in the identified materials, including the globular molecules and the neutral molecules and ions combined with the globular is illustrated in Fig. 3. In total, the materials contain 30 different anionic molecules, 31 cations, and 25 neutral molecules.

Fig. 4 illustrates the seven groups of materials identified, based on the composition and geometry of the globular molecules. Three candidate materials do not fit into any of these categories, they are listed as “Other” in Table II.

Fig. 5 shows that the experimentally measured spontaneous polarizations^{3,16,27,28,32–38,59} agree well with previously reported values for plastic molecular and plastic ionic molecular crystals, but computed values are often slightly higher than the experimental. Extrinsic effects such as defects, grain orientation and boundaries, and electronic leakage can reduce the experimental sponta-

TABLE I: Overview of earlier reported plastic ferroelectrics found in the CSD screening, including Curie and melting temperatures, T_c and T_m [K], coercive field E_c [kV/cm], experimental and computed spontaneous polarization, $P_{\text{exp.}}$ and $P_{\text{calc.}}$ [$\mu\text{C}/\text{cm}^2$], computed electronic bandgap E_g [eV], crystallographic space group, alignment of dipoles, and chemical composition. Melting points are retrieved from the CSD unless a reference is listed. The alignment of dipoles is listed as the angle between molecular dipoles and the polarization axis, as detailed in section III C. For refcode families with more than one hit, the lowest temperature structure is listed.

CSD refcode	T_c	$T_{\text{melt.}}$	E_c	$P_{\text{exp.}}$	$P_{\text{calc.}}$	E_g	Spgr.	Alignment	Chem. comp.
Trimethyl-X-Y									
DIRKEU01 ³²	295 ³²	–	67 ³²	2.0 ³²	5.5	0.3	Pma2	–	(CH ₃) ₄ N ⁺ , FeCl ₄ [–]
Cyclic organic molecules									
RUJBAC ³³	454 ³³	–	–	1.1 ³³	1.7	1.9	P2 ₁	66°, 114°; 36°	2 C ₆ H ₁₂ F ₂ N ⁺ , PbI ₄ ^{2–}
BUJQIJ ²⁷	470 ²⁷	–	10.8 ²⁷	0.48 ²⁷	2.7	4.6	P2 ₁	76°; –	C ₆ H ₁₃ FN ⁺ , I [–]
BUJQOP ²⁷	470 ²⁷	–	9.4 ²⁷	0.40 ²⁷	2.8	4.6	P2 ₁	76°; –	C ₆ H ₁₃ FN ⁺ , I [–]
Dabco-based									
SIWKEP ³⁵	374 ³⁵	–	30 ³⁵	9.0 ³⁵	8.0 ⁵⁸	3.6	Cm	–	C ₆ H ₁₃ N ₂ ⁺ , ReO ₄ [–]
TEDAPC28 ³⁴	378 ¹⁵	–	–	4 ³⁴	5.9	5.2	Pm2 ₁ n	–	C ₆ H ₁₃ N ₂ ⁺ , ClO ₄ [–]
WOLYUR08 ³⁶	374 ³⁶	–	–	5 ³⁶	6.2	5.3	Pm2 ₁ n	–	C ₆ H ₁₃ N ₂ ⁺ , BF ₄ [–]
BILNES ⁵⁹	390 ⁵⁹	–	–	–	15.9	4.5	R3	52°; –	C ₇ H ₁₆ N ₂ ²⁺ , NH ₄ ⁺ , 3 Br [–]
BILNOC ⁵⁹	446 ⁵⁹	–	6-12 ⁵⁹	22 ⁵⁹	21.9	4.0	R3	52°; –	C ₇ H ₁₆ N ₂ ²⁺ , NH ₄ ⁺ , 3 I [–]
Quinuclidinium-based									
LOLHIG02 ²⁸	466 ²⁸	–	–	11.4 ²⁸	12.7 ⁵⁸	4.4	Pn	3°; –	C ₇ H ₁₃ FN ⁺ , ReO ₄ [–]
OROWAV ³	367 ³	–	340 ³	5.2 ³	7.3 ⁵⁸	4.5	Pmn2 ₁	5°; –	C ₇ H ₁₄ N ⁺ , ReO ₄ [–]
YASKIP ¹⁶	322 ¹⁶	–	255 ¹⁶	6.7 ¹⁶	6.5 ⁵⁸	2.9	Pmn2 ₁	6°; –	C ₇ H ₁₄ N ⁺ , IO ₄ [–]
SIYWUT ^{37,60}	–	–	1000 ³⁷	1.7 ³⁷	5.6 ⁵⁸	5.3	P4 ₁	113°; –	C ₇ H ₁₄ NO ⁺ , Cl [–]
ABIQOU ³⁷	–	–	–	–	5.2 ⁵⁸	5.0	P4 ₁	113°; –	C ₇ H ₁₄ NO ⁺ , Br [–]
MIHTEE ³⁸	400 ³⁸	492	–	6.96 ³⁸	10.2	4.6	P6 ₁	85°	(R)–C ₇ H ₁₃ NO
QIVQIY ³⁸	400 ³⁸	–	–	6.72 ³⁸	10.2	4.5	P6 ₅	85°	(S)–C ₇ H ₁₃ NO
Reported non-ferroelectrics									
BOXCUO ⁶¹	–	–	–	–	–	0	P6 ₃ mc	–	C ₄ H ₁₂ P ⁺ , FeCl ₄ [–]
QIMXER ⁶²	–	–	–	–	9.1	4.7	Cmc2 ₁	–	C ₆ H ₁₃ N ₂ ⁺ , Cl [–]
BOBVIY12 ⁶³	–	–	–	–	6.7	3.8	Pmc2 ₁	–	C ₆ H ₁₃ N ₂ ⁺ , I [–]
BOCKEK06 ⁶⁴	–	–	–	–	12.2	4.8	P1	–	C ₆ H ₁₃ N ₂ ⁺ , HF ₂ [–]

neous polarization.^{68,69} Moreover, atomic vibration and molecular librations can also reduce the measured spontaneous polarization. In assessing the properties with DFT, we used the lowest temperature ferroelectric phase reported in CSD, as the dynamic molecular motion could play a significant role at elevated temperatures and in particular in the high-temperature phases. Note that for 44 of the materials, the structure reported at the lowest temperature coincides with the room temperature phase. For four materials, a paraelectric phase is reported at room temperature, and for one material, VAGVAA01, the room temperature structure is a different potentially ferroelectric phase. Finally, for 26 of the materials, no crystalline room temperature phase has been reported in the CSD.

A. Candidate Ferroelectric Plastic Crystals

1. Trimethyl-X-Y materials

One group of plastic ferroelectric candidates is the trimethyl-X-Y materials, where X denotes an atom and Y a chemical group or atom; two structures illustrated in Fig. 4. Out of the 21 materials, only one (DIRKEU01) has previously been reported as ferroelectric. Of the remaining 20, seven are based on neutral molecules, while the rest are constructed from various combinations of 12 anions and seven different cations, the most common being tetramethylammonium, found in 8 out of the 21 materials. This group of materials shows significant promise, with eight having computed spontaneous polarization values exceeding 10 $\mu\text{C}/\text{cm}^2$ (Table II). The largest value is found for VUGNUG with 22 $\mu\text{C}/\text{cm}^2$. For two of the materials, PEVXOE and PEVXUK, we find no bandgap and therefore no spontaneous polar-

TABLE II: Overview of candidate ferroelectric plastic crystals discovered in the screening of the CSD, including melting temperatures T_{melt} [K], computed spontaneous polarization P_{calc} [$\mu\text{C}/\text{cm}^2$], computed electronic bandgap E_g [eV], crystallographic space group, alignment of dipoles and chemical composition. Melting points are retrieved from the CSD unless a reference is listed. T_{struct} is the temperature the structure is measured as, (RT) indicates that the structure is also reported at room temperature. The alignment of dipoles is listed as the angle between molecular dipoles and the polarization axis, as detailed in section III C. For refcode families with more than one hit, the lowest temperature structure is listed.

	CSD refcode	T_{struct}	T_{melt}	P_{calc}	E_g	Spg.	Alignment	Chem. comp.
Trimethyl-X-Y								
M(molecular)	ZZZVPQ01	RT	-	3.0	5.8	R3mr	0°	(CH ₃) ₃ SO ₃ N
	ZZZVPE02	150 (RT)	-	5.4	6.4	R3m	0°	(CH ₃) ₃ BH ₃ N
	LINZOX	RT	-	6.4	4.4	Ama2	63°	(CH ₃) ₃ NH ₃ Al
	TMAMBF11	100 (RT)	367 ¹	20.3	7.4	R3m	0°	(CH ₃) ₃ BF ₃ N
	CAVJOZ	193	-	0.04	2.8	P6 ₂ mc	-	(CH ₃) ₃ Cl ₂ Nb
	TBUHLB05	180	254	7.3	4.9	Pmn2 ₁	19°, 32°, 33°	(CH ₃) ₃ BrC
	ETIPAY	160	183	5.5	5.3	Pna2 ₁	20°	(CH ₃) ₃ CH ₂ ClSi
I(ionic)	WAGGAM	RT	-	11.0	2.7	P2 ₁	6°, 83°;-	2 (CH ₃) ₃ OS ⁺ , Cr ₂ O ₇ ²⁻
	GEPZIK	123	185	3.9	7.6	P6 ₃	-	(CH ₃) ₃ HN ⁺ , F ⁻ , 6 HF
	ZISCUC	300	-	14.4	0.2	Cm	70°;-	(CH ₃) ₃ CH ₂ ClN ⁺ , FeCl ₄ ⁻
	YODGON	RT	-	3.1	5.0	Pmn2 ₁	-	(CH ₃) ₄ N ⁺ , OCN ⁻
	XAKBUG	223	-	15.3	2.6	Abm2	103°;-	(CH ₃) ₄ N ⁺ , OsFO ₄ ⁻
	VUGNUG	RT	-	22.0	5.3	Pmn2 ₁	-	(CH ₃) ₄ N ⁺ , N ₃ ⁻
	MIWBEC	293	-	13.4	0.2	Pca2 ₁	53°;-	(CH ₃) ₄ N ⁺ , FeCl ₃ NO ⁻
	ORUKUK	100	-	12.9	3.0	Pna2 ₁	-	(CH ₃) ₄ N ⁺ , Cl ₃ F ₄ ⁻
	ZOYGUP	RT	484	3.1	4.1	P2 ₁	68°;-	(CH ₃) ₄ N ⁺ , C ₅ H ₇ O ₄ ⁻
	SEYLAJ	123	317	12.1	5.2	P3 ₁	-	(CH ₃) ₄ N ⁺ , OH ⁻ , 4 H ₂ O
	PEVXOE	100	-	-	0	Cmc2 ₁	-	(CH ₃) ₄ P ⁺ , O ₂ ⁻ , 2 NH ₃
	PEVXUK	100	-	-	0	Cmc2 ₁	-	(CH ₃) ₄ As ⁺ , O ₂ ⁻ , 2 NH ₃
XENFAZ	295	493	8.4	1.7	P2 ₁	17°, 161°;-	2 (CH ₂ O) ₃ NH ₃ C ⁺ , HgI ₄ ²⁻	
Dabco-based								
M	LWLWEO	RT	429	7.6	3.4	R3m	18°, 161°;-	C ₆ H ₁₂ N ₂ , 2 CH ₄ N ₂ S
	HUSRES	150	-	8.2	4.8	Cc	-; 14°	C ₆ H ₁₂ N ₂ , C ₂ H ₅ O ₅ P
I	USAFIG	295	-	0.4	3.4	Pna2 ₁	95°;-	C ₆ H ₁₃ N ₂ O ₂ ⁺ , NO ₃ ⁻
	VAGVAA01	150	-	12.8	5.1	Pna2 ₁	-	C ₆ H ₁₄ N ₂ ²⁺ , 2 Cl ⁻
	GASBIO	123	-	11.2	4.2	Pca2 ₁	-	C ₆ H ₁₄ N ₂ ²⁺ , 2 I ⁻ , H ₂ O
	NAKNOF03	150	-	18.4	6.8	P1	-	C ₆ H ₁₄ N ₂ ²⁺ , 2 BF ₄ ⁻ , H ₂ O
Hexamine-based								
M	INEYUY/TAZPAD	100 (RT)	-	0.9	3.8	R3m	0°	C ₆ H ₁₂ N ₃ P
I	HMTAAB	RT	-	11.6	4.8	P6 ₃ mc	-	C ₆ H ₁₂ N ₄ , NH ₄ ⁺ , BF ₄ ⁻
	BOHNUH01	295	-	10.6	4.9	R3m	83°;-	C ₆ H ₁₃ N ₄ ⁺ , Br ⁻
	TOZTAF	296	-	17.3	4.3	Cc	138°; 89°	C ₆ H ₁₃ N ₄ ⁺ , C ₄ H ₅ O ₅ ⁻
Boron clusters								
M	SASSOU	RT	378	8.7	3.5	Cc	80°	CH ₁₀ B ₆ S ₂
	OTOLAM	150	-	11.5	5.5	Pnn2	0°	C ₂ H ₁₄ B ₈
I	UTUZAM	90	-	3.2	4.8	P2 ₁	56°;-	CH ₁₄ B ₉ ⁻ , C ₃ H ₁₀ N ⁺
	LUWHOD	340	-	7.8	4.4	P4 ₂	-	B ₁₀ H ₁₀ ²⁻ , 2 NH ₄ ⁺ , NH ₃
Cyclic organic molecules								
I	WAQBOH	295	-	8.1	5.7	Pn	-	C ₄ H ₁₁ N ₂ ⁺ , BF ₄ ⁻
	CUWZOM	100	-	0.4	5.5	P2 ₁	52°;-	C ₅ H ₁₁ FN ⁺ , Cl ⁻
	AMINIT	293	-	6.8	4.5	P2 ₁	126°; 88°	C ₅ H ₁₂ N ⁺ , H ₂ AsO ₄ ⁻
	EVULAI	100	-	13.2	4.7	P2 ₁	39°	C ₆ H ₁₅ N ₂ S ⁺ , Cl ⁻
	FENYEC	RT	407	4.7	3.5	Cc	55°; 85°	C ₇ H ₅ O ₃ ⁻ , C ₄ H ₁₀ N ⁺
	HAJXEW	123	-	16.5	5.6	Pn	16°;-	C ₆ H ₁₈ N ₃ ³⁺ , ClO ₄ ⁻ , 2 Cl ⁻
	OBEXEY	200	416	7.6	4.8	Cmc2 ₁	-	C ₉ H ₂₀ N ⁺ , N ₃ ⁻

TABLE II: Continuation of Table II

	CSD refcode	T _{struct.}	T _{melt.}	P _{calc.}	E _g	Spg.	Alignment	Chem. comp.
Cage-like organic molecules								
M	EQAXOL	140	–	9.1	5.4	Pna2 ₁	48°	C ₅ H ₉ O ₃ P
	BAPFAB	150	–	4.1	5.3	P2 ₁	20°, 56°	C ₆ H ₇ FO ₃
	BAPFOP	150	–	0.7	5.4	P2 ₁	20°	C ₆ H ₇ FO ₃
	NOCPIE01	100 (RT)	–	14.9	4.5	P2 ₁	51°, 63°	C ₇ H ₁₀ O ₃
	MIRHUQ	180	388 (sublim.)	11.3	4.6	P2 ₁	29°, 31°	C ₈ H ₁₅ PS
	XIBVIN	180	443	1.3	4.2	P2 ₁	77°	C ₈ H ₁₅ PS
	BESWON	130	–	4.5	5.7	P3 ₁	70°	C ₉ H ₁₆ O
	FEJFAB	RT	–	7.4	2.1	Pmc2 ₁	34°;-	C ₆ H ₁₀ N ₂ , CBr ₄
I	PINRAI	173	–	5.3	5.8	Pna2 ₁	60°;-	C ₆ H ₉ F ₃ N ⁺ , Cl ⁻
	QAZFUV	100	–	11.5	5.2	Cmc2 ₁	54°;-	C ₆ H ₁₂ N ⁺ , Cl ⁻
	JEBVOC	293	> 533	8.2	4.4	P2 ₁	70°;-	C ₉ H ₁₄ N ⁺ , Cl ⁻
Other								
I	HUPTUI	100	–	0.4	3.7	P2 ₁	86°; –	C ₆ H ₁₈ N ₃ S ⁺ , TaF ₆ ⁻
	VAJKUM	RT	513	1.7	3.2	P2 ₁	85°; 43°	C ₆ H ₁₈ N ₃ S ⁺ , SF ₅ O ⁻
	OTIJUZ	123	393 ⁶⁵	2.6	5.1	Pc	43°, 120°; –	2 C ₆ H ₁₈ OPSi ⁺ , S ₂ O ₇ ²⁻

ization is listed.

2. Dabco-based Materials

Materials constructed from various derivatives of 1,4-diazabicyclo[2.2.2]octane (dabco) in combinations with anions such as ClO₄⁻ and ReO₄⁻ are attractive ferroelectrics with low coercive fields, and rapid ferroelectric switching reported with frequencies up to 263 kHz.^{23,35,70–72} Moreover, Curie temperatures as high as 540 K have been reported by Li et al.⁷³

In our study, we found 11 dabco-based materials, out of which five have previously been reported as ferroelectrics.^{15,34–36,59} Two of these, BILNES and BILNOC, are organic metal-free perovskites,⁵⁹ see Fig. 4. Interestingly, two of the candidate materials, LOLWEO and HUSRES, are co-crystals of charge-neutral molecules.

The computed spontaneous polarization values for the known ferroelectric dabco-based materials range from 3.56 to 21.9 μC/cm² for BILNOC, compared to 0.4 – 18.4 μC/cm² for the identified candidate ferroelectric plastic crystals.

3. Quinuclidinium-based Materials

Several materials containing variations of the quinuclidinium molecule have been studied in recent years.^{4,13,17,20,37,38,60,74,75} Notably, Tang et al. reported a Curie temperature of 466 K²⁸ for [F–C₇H₁₃N]ReO₄. Another compound of interest is [C₇H₁₄N]IO₄, for which You et al. found 12 equivalent directions of polarization.¹⁶ The reported coercive fields

vary from 255 all the way up to 1000 kV/cm.³⁷ All the seven quinuclidinium-based materials found in our study have previously been reported as ferroelectrics,^{3,16,28,30,37,38,60} (Table I). Five of them are plastic ionic crystals, while the last two are plastic molecular crystals and stereoisomers of the same compound. The computed spontaneous polarizations of the quinuclidinium materials range from 5.2 to 12.7 μC/cm².

4. Hexamine-based Materials

Four hexamine-based crystal structures were identified in the screening study, none of which (to our knowledge) have been reported as ferroelectrics in the past. Fig. 3 shows the two variations of the hexamine molecule found, the regular hexamine molecule, and one where a nitrogen atom has been substituted by phosphorus. Three structures are ionic molecular crystals, with spontaneous polarizations ranging from 10.6 to 18.4 μC/cm² (Table II). One of these, HMTAAB, has a perovskite-like structure, see Fig. 4. The non-ionic molecular crystal with a spontaneous polarization of 0.9 μC/cm² is reported with two refcodes in the CSD, TAZPAD and INEYUY. The large spontaneous polarization values of the ionic hexamine-based materials should encourage further experimental characterization and optimization of this group of materials.

5. Boron Cluster Materials

While boron clusters have been studied for their characteristic chemistry, biological application, as well as

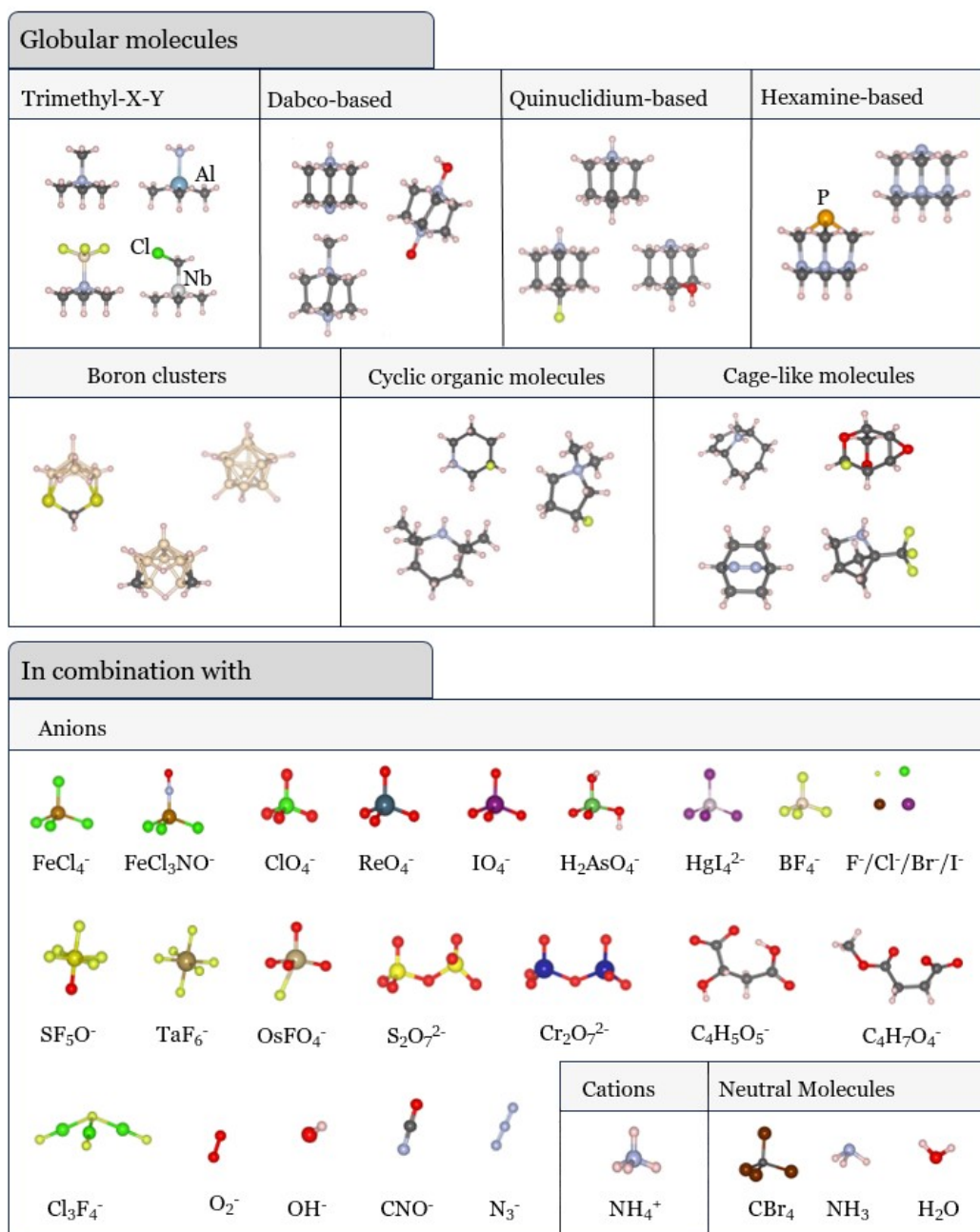


FIG. 3: Examples of globular molecules and the anions, cations, and neutral molecules that are combined in the identified structures. In the top panel, carbon atoms are shown as gray, nitrogen as blue, oxygen as red, fluorine as yellow, boron in beige, and hydrogens as white. Other elements are labeled.

magnetic, optic, and electronic properties,⁷⁶⁻⁷⁹ their ferroelectric properties have not received particular attention. Our screening study identified four materials containing boron clusters (Table II). Two, SASSOU and LUWHOD, are reported at room temperature or higher and have spontaneous polarizations around $8 \mu\text{C}/\text{cm}^2$. The highest polarization is computed for OTOLAM, at $11.5 \mu\text{C}/\text{cm}^2$. The relatively large polarization com-

combined with room temperature stability makes the boron cluster-based materials interesting for further studies.

6. Materials Based on Cyclic Organic Molecules

Some of the crystal structures identified contain cyclic organic molecules, both aromatic or non-aromatic, and

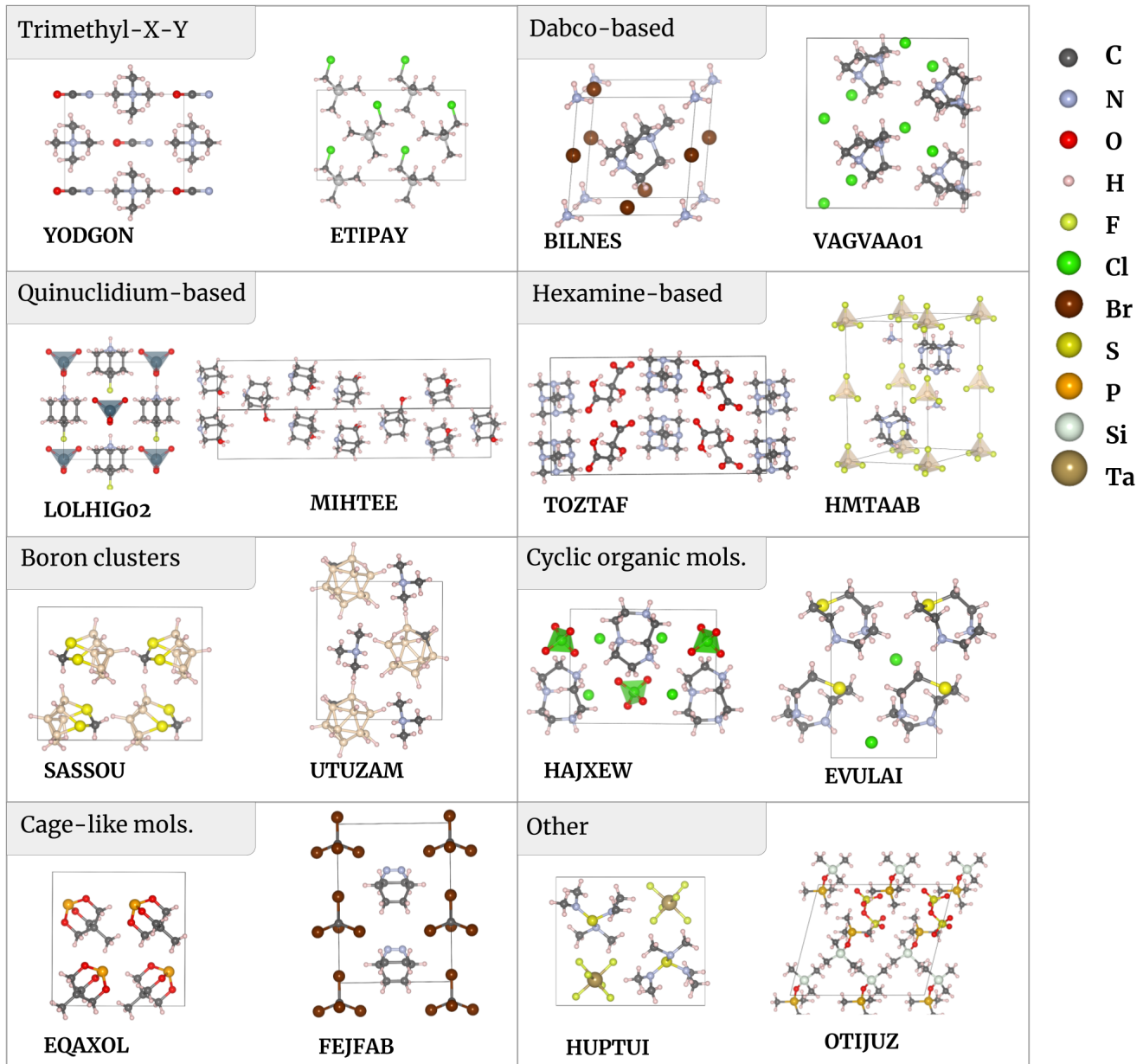


FIG. 4: Examples of structures found in each of the eight groups of materials. ETIPAY, MIHTEE, SASSOU, EQAXOL, and FEJFAB are molecular crystals, the remaining are ionic.

we grouped these together. The 10 materials identified are all ionic molecular crystals including three known ferroelectrics^{27,33} (Table I), two of them being stereoisomers of the same compound. The third, RUJBAC, is an organic-inorganic hybrid perovskite.³³ For all three, the spontaneous polarization fall below $3 \mu\text{C}/\text{cm}^2$. The coercive fields are in the range $10 \text{ kV}/\text{cm}$,²⁷ and they all exhibit Curie temperature exceeding 450 K.^{27,33} Among the seven candidates identified here, all but one have spontaneous polarizations exceeding the earlier reported ferroelectrics, HAJXEW having the largest value

of $16.5 \mu\text{C}/\text{cm}^2$ (Table II). Three of the candidates identified, WAQBOH, AMINIT, and FENYEC have been reported as stable at room temperature, with the latter melting above 400 K.

7. Materials Based on Organic Cage-like Molecules

We found eleven crystals structures with various organic cage-like molecules, none of which have previously been reported as ferroelectric. Seven of these are

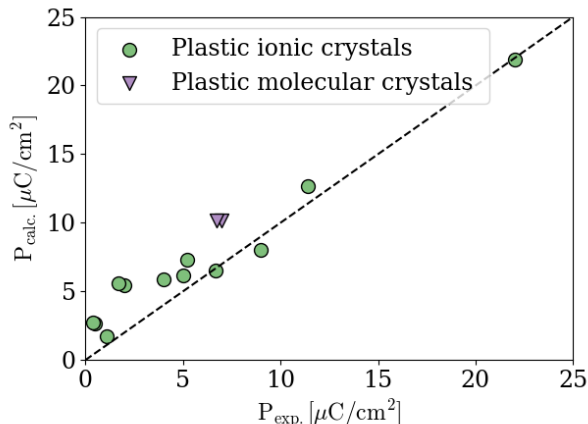


FIG. 5: The computed spontaneous polarization compared with the experimentally measured values. Spontaneous polarization is reported for 14 out of the 16 known ferroelectrics identified in the screening.

molecular crystals, while four are ionic (Table II). Even though there are no reported room temperature structures for MIRHUQ and XIBVIN, their reported sublimation and melting temperatures are high, 388 and 443 K, respectively. Interestingly, these two structures are polymorphs of the same compound. JEBVOC is reported to have a melting temperature larger than 533 K.

Finally, three of the candidate ferroelectrics do not fit into any of the defined groups of materials. The computed spontaneous polarizations are below $3 \mu\text{C}/\text{cm}^2$ for all of them. HUPTUI and VAJKUM are isostructural and are built up of tris(dimethylamino)sulfonium molecule and an octahedral inorganic anion.

B. Comparison of Candidate and Previously Reported Ferroelectrics

The previously reported ferroelectrics frequently contain cage-like organic molecules, such as dabco and quinuclidinium-derivatives, combined with halogen, FeCl_4^- or XO_4^- anions. The molecules in the identified candidates are by comparison generally smaller: 25 materials consist of molecules with five or fewer carbon atoms (not counting structures of boron clusters). The smaller volume of the asymmetric unit allows for larger spontaneous polarization. For example, DIRKEU01 is a known ferroelectric with a computed polarization of $5.5 \mu\text{C}/\text{cm}^2$, VUGNUG is a candidate material with a value of $22.0 \mu\text{C}/\text{cm}^2$. Both materials are of the trimethyl-X-Y group with 0.5 formula units per asymmetric unit, and the cell volume of DIRKEU01 is almost twice as large as VUGNUG. The smaller volume of VUGNUG results in a higher dipole density, and thus the larger spontaneous polarization. The lower molecular weights of the smaller molecules of the candi-

date materials could, however, lead to reduced melting points. Overall, the candidates display a more diverse set of anions that include entities like HF_2^- , CNO^- , FeCl_3NO^- , and SF_5O^- .

C. Polarization and Alignment of Molecules

Molecules in plastic crystals often pack in complex arrangements, and the direction of the individual molecular dipoles does not necessarily align with the direction of the spontaneous polarization.⁵⁸ In Table I and II, the “dipolar” direction relative to the polarization direction is listed. Typically, the unit cell holds several equivalent molecules that align at the same angle with the polarization axis, as given by the space group symmetry. Mirror and/or rotational symmetries cause the polarization contributions perpendicular to the polarization axis to cancel out. For many of the molecules, the dipolar direction is evident from their symmetry, but not all molecules have a clear direction. We therefore conveniently obtain the “dipole” direction from the moments of the electronegativity relative to the center of electronegativity.

Fig. 6 illustrates the alignment of the molecular dipoles relative to the polarization axis for MIWBEC. In the cases where the molecules are symmetrical or have a negligible dipole, no alignment is listed. In these materials, interspecies charge transfer is the dominant contribution to the spontaneous polarization. Examples of such systems, are six of the dabco-based materials, SIWKEP, TEDAPC28, WOLYUR08, VAGVAA01, GASBIO, and NAKNOF03. Despite negligible molecular dipoles, their spontaneous polarizations are in the range $5.0 - 18.4 \mu\text{C}/\text{cm}^2$. For systems where the molecular dipoles run counter to the overall polarization, an interesting prospect opens up for realignment of the dipoles by applying an electric field. This can both increase the spontaneous polarization and allow for multi-bit storage, assuming that the electric field required to realign the dipoles is smaller than the coercive field of the ferroelectric material.

D. Plastic Properties of the Candidate Ferroelectrics

While the screening study can identify candidate ferroelectric plastic crystals, truly predicting whether the materials can transition to a plastic mesophase demands more involved simulations such as molecular dynamics. This is not feasible for the large pool of candidate materials identified in this study, but out of the 16 identified known ferroelectrics, 11 are reported to be plastic crystals.^{3,16,23,28,32,37,38,80} Furthermore, the high-temperature phases of BUJQIJ and BUJQOP have not been solved due to poor XRD data,²⁷ which can indicate the high degree of disorder typical for plastic crystals. This shows that the screening procedure is suited

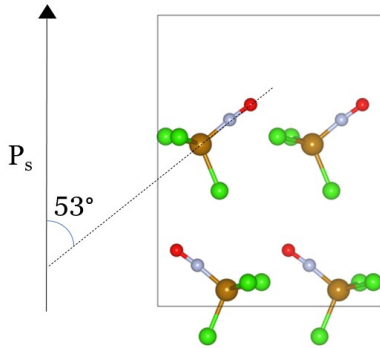


FIG. 6: Illustration of the alignment of dipoles in MIWBEC (tetramethylamine molecules omitted for simplicity). The dipoles align along two directions, both 53° on the polarization axis.

to identify materials with plastic properties and orientationally disordered mesophases.

To identify plastic crystals amongst the candidate materials, we look to the CSD. We both investigated all structures within each refcode family and performed a structure search using Conquest⁸¹ to find plastic phases reported with a different refcode. Three candidate materials were identified as plastic crystals where all molecules exhibit rotational disorder, namely TMAMBF11,¹ ZZZVPE02,¹ and ZISCUC.⁸² LOLWEO has a reported high-temperature phase where one of the two molecular constituents shows rotational disorder. It can be noted that no reported plastic phase does not necessarily indicate that the material is not plastic – only that no plastic phase has been studied.

E. Cohesive Energy and Thermal Stability

For device applications, thermal stability is an important property, and operational temperatures should be significantly below melting and sublimation temperatures. The melting temperature of plastic crystals can be higher than for similar ionic and molecular crystals. As these materials transition into a plastic mesophase, the orientational disorder and increased freedom of movement increase the entropy, making it less favorable to melt due to the reduced entropy gain, as first reported by Timmermans⁹. The volume change at the phase transition is also small.⁸³ In some cases, the reduced entropy gain can make sublimation more favorable than melting. A high Curie temperature is also a prerequisite for ferroelectric and piezoelectric applications.

For 44 out of the 75 materials identified in this study, the CSD entry concerns an ordered structure obtained at ambient temperature. The fraction of room temperature investigations is highest for ionic crystals, Fig. 7, a result that is in line with the higher stability of the ionic

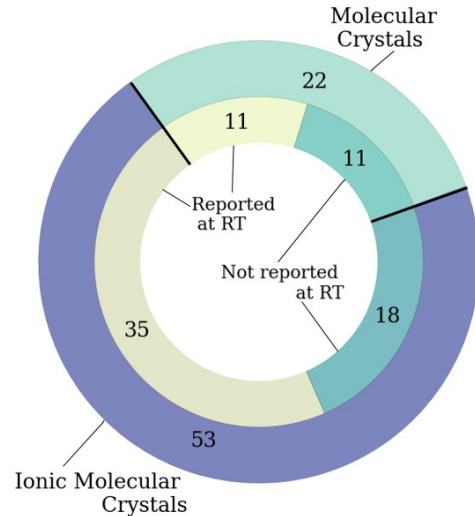


FIG. 7: Overview of the molecular and ionic molecular crystals identified. The outer ring indicates the number of materials, and the inner ring indicates if the potentially ferroelectric phase is reported at room temperature.

molecular crystals, due to electrostatic interactions.

To further investigate the cohesion of molecular crystals, we compute the cohesive energies of XIBVIN and MIRHUQ. These materials are polymorphs of the same compound, differing only by their alignment of molecules, see Fig. 8. XIBVIN has a low degree of alignment of 77° , combined with a low spontaneous polarization of $1.3 \mu\text{C}/\text{cm}^2$. MIRHUQ shows better alignment, with angles of 29° and 31° , and as one could expect, a higher spontaneous polarization of $11.3 \mu\text{C}/\text{cm}^2$. While the larger polarization of MIRHUQ makes it more interesting as a ferroelectric, it is reported to sublimate at 388 K, while XIBVIN melts at 443 K. The computed values for the cohesive energies are $0.26 \text{ eV}/\text{molecule}$ for MIRHUQ and $0.30 \text{ eV}/\text{molecule}$ for XIBVIN, the larger value corresponding to the less aligned structure with the highest melting point. The difference in thermal stability also indicates that at most one of the structures has a plastic phase. If both structures transitioned into rotationally disordered plastic mesophase, it could be assumed that the plastic phases had similar structures, and thus similar phase transition temperatures and mechanisms. The higher phase transition temperature of XIBVIN indicates that this structure transitions into a plastic mesophase, as the entropy gain in such transition can stabilize the solid phase.

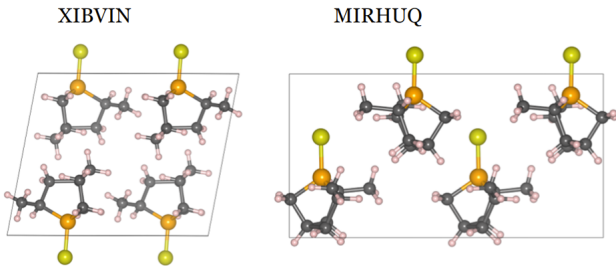


FIG. 8: The two crystal structures of $C_8H_{15}PS$ identified in the screening. The alignment of dipoles differs in the two structures, with a low degree of alignment in XIBVIN, and better alignment in MIRHUQ.

F. Electronic Band Gap and Multisource Energy Harvesting

Ferroelectric materials with band gaps in the visible range can be of particular interest, as these can be promising for application in multi-source energy harvesting devices where piezo- or pyroelectric energy harvesting is combined with the harvesting of solar energy.^{84,85} Therefore, we computed the band gaps for all identified materials to find those that could be suitable for such applications.

Tables I and II lists the computed band gaps. As the computations were performed using the vdW-DF-cx functional, which describes exchange at the generalized-gradient approximation level,⁵⁷ we expect the values to be underestimated. Three materials are predicted to not have a band gap, this was confirmed using the hybrid functional HSE06. Most of the computed band gaps exceed 4 eV; however, six materials have values smaller than 2 eV. Four of these belong to Trimethyl-X-Y group, which would be interesting for multi-source energy harvesting.

G. Design Strategies for Ferroelectric Plastic Crystals

Novel and improved ferroelectric plastic crystals can be engineered by making new combinations of molecular species. As such, the various species found in the various plastic crystal candidates can be used as building blocks for novel material design, a selection of these are displayed in Fig. 3.

Of particular interest are substitutions that are likely to result in similar or isostructural materials. For systems where this is possible, solid-solution engineering can be used to tweak material properties. Three examples of pairs of candidates for such alterations are found among the trimethyl-X-Y materials. The compositions between each pair of materials are similar, only differing by the substitution of molecules with similar geometries. PEVXOE and PEVXUK are isostruc-

tural and only differ by the substitution of $(CH_3)_4P^+$ for $(CH_3)_4As^+$. For ZZZVPE02 and TMAMBF11, the substitution of $(CH_3)_3BH_3N$ to $(CH_3)_3BF_3N$ yields an isostructural material where the spontaneous polarization is increased from 5.4 to 20.3 $\mu C/cm^2$. A similar effect is seen for YODGON and VUGNUG, where the substitution of OCN^- for N_3^- leads to an increase in the spontaneous polarization from 6.4 to 22.0 $\mu C/cm^2$.

Another example of substitution resulting in similar packing is the earlier reported ferroelectrics TEDAPC28 and SIWKEP, which consist of a dabco molecule and ClO_4^- or ReO_4^- , respectively. Such a substitution somewhat changes the orientation of molecules, resulting in a different space group. Whereas the ReO_4^- material has a computed spontaneous polarization of 8 $\mu C/cm^2$, while the ClO_4^- analog has a value of 5.9 $\mu C/cm^2$. The screening identified ten different tetrahedral inorganic anions, but other options also exist and can be considered for the design of new ferroelectric plastic crystals.

Substitutions of single atoms in the organic globular molecule can also be a route to engineer the ferroelectric properties.⁸⁶ For instance, Lin et al. substituted a hydrogen atom in tetramethylammonium for the halogens I, Cl, and Br. The crystal structure was retained, while the number of ferroelectric polar axes increased from 2 for iodine to 6 for chlorine.⁸⁷

IV. CONCLUSIONS

Using a CSD-based workflow, we have identified 55 candidate ferroelectric plastic crystals. The 21 with spontaneous polarization exceeding 10 $\mu C/cm^2$ are arguably the ones with the most potential in ferroelectric devices. Among these, eight in the trimethyl-X-Y group also display a large variation in electronic band gaps that could make them useful also for multi-source energy harvesting.

Our study has successfully identified a range of candidate ferroelectric plastic crystals, including 16 that have been reported as ferroelectrics in the past. The screening criteria used were quite strict, and relaxing some of them, such as the size limitations on both molecules and unit cells, would have expanded the pool. The criteria were based on the previously reported ferroelectric plastic crystals. For this reason, crystal structures that differ significantly from the earlier reported ones could have been overlooked. Still, the identification of the boron cluster-based materials was unexpected, illustrating the potency of the CSD screening. In the design of novel ferroelectric plastic crystals, a good starting point is combining different globular molecular species, i.e., combinations of cations and anions. The various molecular species in the materials identified here, and the corresponding crystal structures, can serve as inspiration for such design.

In this study, we have not assessed whether the polarizations of the candidate ferroelectrics are switchable,

which is a criterion for ferroelectricity. However, all the candidate materials will have pyro- and piezoelectric properties due to their crystal symmetries. This study and the identified compounds should stimulate further theoretical or experimental studies, to assess their ferroelectric switchability, and other characteristics such as the Curie temperatures, and material stability.

V. DATA AVAILABILITY

All the relaxed crystal structures used in this study can be accessed through the NOMAD database at <https://dx.doi.org/10.17172/NOMAD/2023.06.12-1>. All other data is available upon reasonable request.

ACKNOWLEDGMENTS

The computations of this work were carried out on UNINETT Sigma2 high-performance computing resources (grant NN9650K). This work is supported by the Research Council of Norway as a part of the Young Research Talent project FOX (302362). Structure and molecule figures are made using the software programs Mercury and VESTA.

Appendix A: Molecular Graph Theory

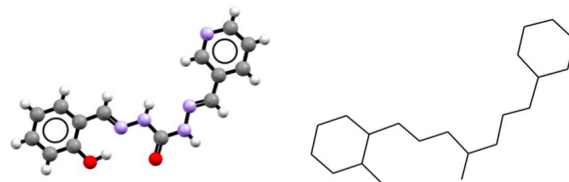


FIG. 9: Illustration of a network representation of a molecule. The network only considers the connectivity, as given by covalent bonds between atoms. Hydrogen atoms are omitted when constructing the molecular graph.

A graph, or network, consists of a set of nodes that can be connected by edges.⁸⁸ Fig. 9 illustrates this in the context of a molecule. A covalently bonded molecule is represented as a graph, with atoms as nodes and covalent bonds as edges. A node with two edges is called a chain and if a part of a graph can become disconnected by cutting one single chain, it is called a bridge. To avoid long, flexible molecules that are unlikely to rotate, we required molecules to have at most two connected bridge nodes, i.e., the molecule shown in Fig. 9 was excluded due to a high number of connected bridges.

-
- [1] A. Mondal, B. Bhattacharya, S. Das, S. Bhunia, R. Chowdhury, S. Dey, and C. M. Reddy, Metal-like Ductility in Organic Plastic Crystals: Role of Molecular Shape and Dihydrogen Bonding Interactions in Aminoboranes, *Angew. Chem. Int. Ed.* **59**, 10971 (2020).
- [2] S. Saha, M. K. Mishra, C. M. Reddy, and G. R. Desiraju, From Molecules to Interactions to Crystal Engineering: Mechanical Properties of Organic Solids, *Acc. Chem. Res.* **51**, 2957 (2018).
- [3] J. Harada, T. Shimojo, H. Oyamaguchi, H. Hasegawa, Y. Takahashi, K. Satomi, Y. Suzuki, J. Kawamata, and T. Inabe, Directionally tunable and mechanically deformable ferroelectric crystals from rotating polar globular ionic molecules, *Nat. Chem.* **8**, 946 (2016).
- [4] S. Deng, J. Li, X. Chen, Y. Hou, and L. Chen, A novel ferroelectric based on quinuclidine derivatives, *Chin. Chem. Lett.* **31**, 1686 (2020).
- [5] X. Lan, X. Wang, D. X. Zhang, T. Mu, and X. Z. Lan, Cation and Anion Transfer in Quinuclidinium Hexafluorophosphate Plastic Crystal: Role of Constituent Ions and the Crystalline Structure, *J. Phys. Chem. C* **125**, 21169 (2021).
- [6] M. Owczarek, K. A. Hujsak, D. P. Ferris, A. Prokofjevs, I. Majerz, P. Szklarz, H. Zhang, A. A. Sarjeant, C. L. Stern, R. Jakubas, S. Hong, V. P. Dravid, and J. F. Stoddart, Flexible ferroelectric organic crystals, *Nat. Commun.* **7**, 13108 (2016).
- [7] J. Walker, S. Scherrer, N. S. Løndal, T. Grande, and M.-A. Einarsrud, Electric field dependent polarization switching of tetramethylammonium bromotrichloroferrate(III) ferroelectric plastic crystals, *Appl. Phys. Lett.* **116**, 242902 (2020).
- [8] Y. Hu, J. L. Gottfried, R. Pesce-Rodriguez, C.-C. Wu, S. D. Walck, Z. Liu, S. Balakrishnan, S. Broderick, Z. Guo, Q. Zhang, L. An, R. Adlakha, M. Nouh, C. Zhou, P. W. Chung, and S. Ren, Releasing chemical energy in spatially programmed ferroelectrics, *Nat. Commun.* **13**, 6959 (2022).
- [9] J. Timmermans, Plastic crystals: A historical review, *J. Phys. Chem. Solids* **18**, 1 (1961).
- [10] H. Ishida, T. Iwachido, N. Hayama, R. Ikeda, M. Hashimoto, and D. Nakamura, Structural Phase Transitions in Solid tert-Butylammonium Nitrate as Studied by Differential Thermal Analysis and ¹H-NMR, *Z. Naturforsch. A* **44**, 71 (1989).
- [11] J. M. Pringle, Recent progress in the development and use of organic ionic plastic crystal electrolytes, *Phys. Chem. Chem. Phys.* **15**, 1339 (2013).
- [12] Z.-H. Wei, Z.-T. Jiang, X.-X. Zhang, M.-L. Li, Y.-Y. Tang, X.-G. Chen, H. Cai, and R.-G. Xiong, Rational Design of Ceramic-Like Molecular Ferroelectric by Quasi-Spherical Theory, *J. Am. Chem. Soc.* **142** (2020).

- [13] H.-Y. Zhang, Y.-Y. Tang, P.-P. Shi, and R.-G. Xiong, Toward the Targeted Design of Molecular Ferroelectrics: Modifying Molecular Symmetries and Homochirality, *Acc. Chem. Res.* **52**, 1928 (2019).
- [14] A. Olejniczak, M. Anioła, M. Szafranski, A. Budzianowski, and A. Katrusiak, New Polar Phases of 1,4-Diazabicyclo[2.2.2]octane Perchlorate, An NH⁺...N Hydrogen-Bonded Ferroelectric, *Crystal Growth & Design* **13**, 2872 (2013).
- [15] A. Olejniczak, M. Szafranski, and A. Katrusiak, Pressure-Temperature Phase Diagrams and Transition Mechanisms of Hybrid Organic-Inorganic NH...N Bonded Ferroelectrics, *Cryst. Growth Des.* **18**, 6488 (2018).
- [16] Y.-M. You, Y.-Y. Tang, P.-F. Li, H.-Y. Zhang, W.-Y. Zhang, Y. Zhang, H.-Y. Ye, T. Nakamura, and R.-G. Xiong, Quinuclidinium salt ferroelectric thin-film with duodecuple-rotational polarization-directions, *Nat. Commun.* **8**, 14934 (2017).
- [17] Y. Xie, Y. Ai, Y.-L. Zeng, W.-H. He, X.-Q. Huang, D.-W. Fu, J.-X. Gao, X.-G. Chen, and Y.-Y. Tang, The Soft Molecular Polycrystalline Ferroelectric Realized by the Fluorination Effect, *J. Am. Chem. Soc.* **142**, 12486 (2020).
- [18] B. Wang, D. Ma, H. Zhao, L. Long, and L. Zheng, Room Temperature Lead-Free Multiaxial Inorganic-Organic Hybrid Ferroelectric, *Inorg. Chem.* **58**, 13953 (2019).
- [19] S. Das, A. Mondal, and C. M. Reddy, Harnessing molecular rotations in plastic crystals: a holistic view for crystal engineering of adaptive soft materials, *Chem. Soc. Rev.* **49**, 8878 (2020).
- [20] C.-K. Yang, W.-N. Chen, Y.-T. Ding, J. Wang, Y. Rao, W.-Q. Liao, Y. Xie, W. Zou, and R.-G. Xiong, Directional Intermolecular Interactions for Precise Molecular Design of a High- T_c Multiaxial Molecular Ferroelectric, *J. Am. Chem. Soc.* **141**, 1781 (2019).
- [21] J. Harada, Plastic/ferroelectric molecular crystals: Ferroelectric performance in bulk polycrystalline forms, *APL Mater.* **9**, 020901 (2021).
- [22] Y. Ai, Y.-L. Zeng, W.-H. He, X.-Q. Huang, and Y.-Y. Tang, Six-Fold Vertices in a Single-Component Organic Ferroelectric with Most Equivalent Polarization Directions, *J. Am. Chem. Soc.* **142**, 13989 (2020).
- [23] Y.-Y. Tang, P.-F. Li, W.-Y. Zhang, H.-Y. Ye, Y.-M. You, and R.-G. Xiong, A Multiaxial Molecular Ferroelectric with Highest Curie Temperature and Fastest Polarization Switching, *J. Am. Chem. Soc.* **139**, 13903 (2017).
- [24] Y. Zhang, X.-J. Song, Z.-X. Zhang, D.-W. Fu, and R.-G. Xiong, Piezoelectric Energy Harvesting Based on Multiaxial Ferroelectrics by Precise Molecular Design, *Matter* **2**, 697 (2020).
- [25] Z. Zafar, A. Zafar, X. Guo, Q. Lin, and Y. Yu, Raman evolution of order-disorder phase transition in multiaxial molecular ferroelectric thin film, *J Raman Spectrosc* **50**, 1576 (2019).
- [26] Y.-Y. Tang, P.-F. Li, W.-Q. Liao, P.-P. Shi, Y.-M. You, and R.-G. Xiong, Multiaxial Molecular Ferroelectric Thin Films Bring Light to Practical Applications, *J. Am. Chem. Soc.* **140**, 8051 (2018).
- [27] Y. Ai, D.-J. Wu, M.-J. Yang, P. Wang, W.-H. He, and W.-Q. Liao, Highest- T_c organic enantiomeric ferroelectrics obtained by F/H substitution, *Chem. Commun.* , 7033 (2020).
- [28] Y.-Y. Tang, Y. Xie, Y. Ai, W.-Q. Liao, P.-F. Li, T. Nakamura, and R.-G. Xiong, Organic Ferroelectric Vortex-Antivortex Domain Structure, *J. Am. Chem. Soc.* **142**, 21932 (2020).
- [29] L. Baudry, I. Lukyanchuk, and V. M. Vinokur, Ferroelectric symmetry-protected multibit memory cell, *Sci. Rep.* **7**, 42196 (2017).
- [30] J. Harada, Y. Kawamura, Y. Takahashi, Y. Uemura, T. Hasegawa, H. Taniguchi, and K. Maruyama, Plastic/Ferroelectric Crystals with Easily Switchable Polarization: Low-Voltage Operation, Unprecedentedly High Pyroelectric Performance, and Large Piezoelectric Effect in Polycrystalline Forms, *J. Am. Chem. Soc.* **141**, 9349 (2019).
- [31] R. E. Cohen, Origin of ferroelectricity in perovskite oxides, *Nature* **358**, 136 (1992).
- [32] J. Harada, N. Yoneyama, S. Yokokura, Y. Takahashi, A. Miura, N. Kitamura, and T. Inabe, Ferroelectricity and piezoelectricity in free-standing polycrystalline films of plastic crystals, *J. Am. Chem. Soc.* **140**, 346 (2018).
- [33] X.-G. Chen, X.-J. Song, Z.-X. Zhang, H.-Y. Zhang, Q. Pan, J. Yao, Y.-M. You, and R.-G. Xiong, Confinement-Driven Ferroelectricity in a Two-Dimensional Hybrid Lead Iodide Perovskite, *J. Am. Chem. Soc.* **142**, 10212 (2020).
- [34] Y.-Y. Tang, W.-Y. Zhang, P.-F. Li, H.-Y. Ye, Y.-M. You, and R.-G. Xiong, Ultrafast polarization switching in a biaxial molecular ferroelectric thin film: [hdabco]clo₄, *J. Am. Chem. Soc.* **138**, 15784 (2016).
- [35] M. Szafranski, A. Katrusiak, and G. J. McIntyre, Ferroelectric Order of Parallel Bistable Hydrogen Bonds, *Phys. Rev. Lett.* **89**, 215507 (2002).
- [36] A. Budzianowski and A. Katrusiak, Anomalous Protonic-Glass Evolution from Ordered Phase in NH⁺...N Hydrogen-Bonded DabcoHBF₄ Ferroelectric, *J. Phys. Chem. B* , 7 (2008).
- [37] P.-F. Li, Y.-Y. Tang, Z.-X. Wang, H.-Y. Ye, Y.-M. You, and R.-G. Xiong, Anomalous rotary polarization discovered in homochiral organic ferroelectrics, *Nat. Commun.* **7**, 13635 (2016).
- [38] P.-F. Li, W.-Q. Liao, Y.-Y. Tang, W. Qiao, D. Zhao, Y. Ai, Y.-F. Yao, and R.-G. Xiong, Organic enantiomeric high- T_c ferroelectrics, *Proc. Natl. Acad. Sci. U.S.A.* **116**, 5878 (2019).
- [39] S. Horiuchi and S. Ishibashi, Hydrogen-Bonded Small-Molecular Crystals Yielding Strong Ferroelectric and Antiferroelectric Polarizations, *J. Phys. Soc. Jpn.* **89**, 051009 (2020).
- [40] G. C.r, B. I.j, L. M.p, and W. S.c, The Cambridge Structural Database, *Acta Crystallogr. B: Struct. Sci. Cryst. Eng. Mater.* **72**, 171 (2016).
- [41] S. Seyedraoufi, E. D. Sødahl, C. H. Görbitz, and K. Berland, Database mining and first-principles assessment of organic proton-transfer ferroelectrics (2023), arXiv:2306.00363.
- [42] K. Berland, E. D. Sødahl, and S. Seyedraoufi, *Molcrys*, <https://gitlab.com/m7582/molcrys/> (2023).
- [43] A. H. Larsen, J. J. Mortensen, J. Blomqvist, I. E. Castelli, R. Christensen, M. Dułak, J. Friis, M. N. Groves, B. Hammer, C. Hargus, E. D. Hermes, P. C. Jennings, P. B. Jensen, J. Kermode, J. R. Kitchin, E. L. Kolsbjerg, J. Kubal, K. Kaasbjerg, S. Lysgaard, J. B. Maronsson, T. Maxson, T. Olsen, L. Pastewka, A. Peterson, C. Rostgaard, J. Schiøtz, O. Schütt, M. Strange, K. S. Thygesen, T. Vegge, L. Vilhelmsen, M. Walter, Z. Zeng, and K. W. Jacobsen, The atomic simulation environment—a python library for working with atoms, *J. Condens. Matter Phys.* **29**, 273002 (2017).
- [44] A. Hagberg, P. Swart, and D. S Chult, Exploring net-

- work structure, dynamics, and function using networkx, (2008).
- [45] Y. Zhang, W. Zhang, S.-H. Li, Q. Ye, H.-L. Cai, F. Deng, R.-G. Xiong, and S. D. Huang, Ferroelectricity Induced by Ordering of Twisting Motion in a Molecular Rotor, *J. Am. Chem. Soc.* **134**, 11044 (2012).
- [46] D. André, A. Dworkin, H. Szwarc, R. Céolin, V. Agafonov, C. Fabre, A. Rassat, L. Straver, P. Bernier, and A. Zahab, Molecular packing of fullerene C₆₀ at room temperature, *Mol. Phys.* **76**, 1311 (1992).
- [47] T. E. Jenkins and J. Lewis, A Raman study of adamantane (C₁₀H₁₆), diamantane (C₁₄H₂₀) and triamantane (C₁₈H₂₄) between 10 K and room temperatures, *Spectrochim. Acta, Part A* **36**, 259 (1980).
- [48] D. Szweczyk, A. Jeżowski, A. I. Krivchikov, and J. L. Tamarit, Influence of thermal treatment on thermal properties of adamantane derivatives, *Low Temp. Phys.* **41**, 469 (2015).
- [49] G. Kresse and J. Hafner, *Ab initio* molecular-dynamics simulation of the liquid-metal–amorphous-semiconductor transition in germanium, *Phys. Rev. B* **49**, 14251 (1994).
- [50] G. Kresse and J. Hafner, *Ab initio* molecular dynamics for liquid metals, *Phys. Rev. B* **47**, 558 (1993).
- [51] G. Kresse and J. Furthmüller, Efficiency of *ab-initio* total energy calculations for metals and semiconductors using a plane-wave basis set, *Comput. Mater. Sci.* **6**, 15 (1996).
- [52] G. Kresse and J. Furthmüller, Efficient iterative schemes for *ab initio* total-energy calculations using a plane-wave basis set, *Phys. Rev. B* **54**, 11169 (1996).
- [53] P. E. Blöchl, Projector augmented-wave method, *Phys. Rev. B* **50**, 17953 (1994).
- [54] G. Kresse and D. Joubert, From ultrasoft pseudopotentials to the projector augmented-wave method, *Phys. Rev. B* **59**, 1758 (1999).
- [55] R. Resta, Macroscopic polarization in crystalline dielectrics: the geometric phase approach, *Rev. Mod. Phys.* **66**, 899 (1994).
- [56] S. Baroni and R. Resta, *Ab initio* calculation of the macroscopic dielectric constant in silicon, *Phys. Rev. B* **33**, 7017 (1986).
- [57] K. Berland and P. Hyldgaard, Exchange functional that tests the robustness of the plasmon description of the van der Waals density functional, *Phys. Rev. B* **89**, 035412 (2014).
- [58] E. D. Sødahl, J. Walker, and K. Berland, Piezoelectric Response of Plastic Ionic Molecular Crystals: Role of Molecular Rotation, *Cryst. Growth Des.* **23**, 729 (2023).
- [59] H.-Y. Ye, Y.-Y. Tang, P.-F. Li, W.-Q. Liao, J.-X. Gao, X.-N. Hua, H. Cai, P.-P. Shi, Y.-M. You, and R.-G. Xiong, Metal-free three-dimensional perovskite ferroelectrics, *Science* **361**, 151 (2018).
- [60] M. Siczek and T. Lis, (r)-(-)-3-hydroxy-quinuclidinium chloride, *Acta Cryst. E* **64**, 842 (2008).
- [61] P.-P. Shi, Q. Ye, Q. Li, H.-T. Wang, D.-W. Fu, Y. Zhang, and R.-G. Xiong, Novel Phase-Transition Materials Coupled with Switchable Dielectric, Magnetic, and Optical Properties: [(CH₃)₄P][FeCl₄] and [(CH₃)₄P][FeBr₄], *Chem. Mater.* **8** (2014).
- [62] M. Szafranski, Strong negative thermal expansion and relaxor ferroelectricity driven by supramolecular patterns, *J. Mater. Chem. C* **1**, 7904 (2013).
- [63] A. Olejniczak, A. Katrusiak, and M. Szafranski, Ten polymorphs of nh⁺⋯n hydrogen-bonded 1,4-diazabicyclo[2.2.2]octane complexes: Supramolecular origin of giant anisotropic dielectric response in polymorph v, *Cryst. Growth Des.* **10**, 3537 (2010).
- [64] M. Szafranski, Temperature-induced displacement of the proton site in strong f–h–f hydrogen bond and mechanism of phase transition in 1,4 diazabicyclo[2.2.2]octane dihydrogen difluoride, *Chem. Phys. Lett.* **457**, 110 (2008).
- [65] K. Bläsing, R. Labbow, A. Schulz, and A. Villinger, Silylated sulfuric acid: Preparation of a tris(trimethylsilyl)oxosulfonium [(me₃si-o)₃so]⁺ salt, *Angew. Chem. Int. Ed.* **60**, 13798 (2021).
- [66] A. Budzianowski and A. Katrusiak, Pressure tuning between nh⁺⋯n hydrogen-bonded ice analogue and nh⁺⋯br polar dabcohr complexes, *J. Phys. Chem. B* **110**, 9755 (2006).
- [67] A. V. Krukau, O. A. Vydrov, A. F. Izmaylov, and G. E. Scuseria, Influence of the exchange screening parameter on the performance of screened hybrid functionals, *J. Chem. Phys.* **125**, 224106 (2006).
- [68] M. Maglione, G. Philippot, D. Lévassieur, S. Payan, C. Aymonier, and C. Elissalde, Defect chemistry in ferroelectric perovskites: long standing issues and recent advances, *Dalton Trans.* **44**, 13411 (2015).
- [69] D. Damjanovic, Ferroelectric, dielectric and piezoelectric properties of ferroelectric thin films and ceramics, *Rep. Prog. Phys.* **61**, 1267 (1998).
- [70] Z. Sun, X. Yi, K. Tao, C. Ji, X. Liu, L. Li, S. Han, A. Zheng, M. Hong, and J. Luo, A Molecular Ferroelectric Showing Room-Temperature Record-Fast Switching of Spontaneous Polarization, *Angew. Chem.* **130**, 9981 (2018).
- [71] Y.-Y. Tang, W.-Y. Zhang, P.-F. Li, H.-Y. Ye, Y.-M. You, and R.-G. Xiong, Ultrafast Polarization Switching in a Biaxial Molecular Ferroelectric Thin Film: [Hdabco]ClO₄, *J. Am. Chem. Soc.* **138**, 15784 (2016).
- [72] D.-W. Fu, J.-X. Gao, W.-H. He, X.-Q. Huang, Y.-H. Liu, and Y. Ai, High-Tc Enantiomeric Ferroelectrics Based on Homochiral Dabco-derivatives (Dabco=1,4-Diazabicyclo[2.2.2]octane), *Angew. Chem. Int. Ed.* **59**, 17477 (2020).
- [73] J.-Y. Li, Q.-L. Xu, S.-Y. Ye, L. Tong, X. Chen, and L.-Z. Chen, A multiaxial molecular ferroelectric with record high T_c designed by intermolecular interaction modulation, *Chem. Commun.* **57**, 943 (2021).
- [74] M. Yoneya and J. Harada, Molecular Dynamics Simulation Study of the Plastic/Ferroelectric Crystal Quinuclidinium Perrhenate, *J. Phys. Chem. C* **124**, 2171 (2020).
- [75] J. Lee, W. Seol, G. Anoop, S. Samanta, S. Unithrattil, D. Ahn, W. Kim, G. Jung, and J. Jo, Stabilization of Ferroelectric Phase in Highly Oriented Quinuclidinium Perrhenate (HQReO₄) Thin Films, *Materials* **14**, 2126 (2021).
- [76] J. L. Li and G. W. Yang, Iron Endohedral-Doped Boron Fullerene: A Potential Single Molecular Device with Tunable Electronic and Magnetic Properties, *J. Phys. Chem. C* **113**, 18292 (2009).
- [77] L. Ma, H. He, B.-F. Yang, Q. Zhang, and G.-Y. Yang, [Pb(en)_{0.5}][B₅O₈(OH)]: A New Bilayered Organic–Inorganic Hybrid Lead Borate Built by B₅O₈(OH) Cluster Units, *J. Clust. Sci.* **26**, 1495 (2015).
- [78] D. Zhao, X. He, M. Li, B. Wang, C. Guo, C. Rong, P. K. Chattaraj, and S. Liu, Density functional theory studies of boron clusters with exotic properties in bonding, aromaticity and reactivity, *Phys. Chem. Chem. Phys.* **23**, 24118 (2021).
- [79] A. Barba-Bon, G. Salluce, I. Lostalé-Seijo, K. I. Assaf,

- A. Hennig, J. Montenegro, and W. M. Nau, Boron clusters as broadband membrane carriers, *Nature* **603**, 637 (2022).
- [80] A. Katrusiak, Proton dynamics in NH⁺-N hydrogen bond in the paraelectric structure of 1,4-diazabicyclo[2.2.2]octane perchlorate, *J. Mol. Struct.* **552**, 159 (2000).
- [81] I. J. Bruno, J. C. Cole, P. R. Edgington, M. Kessler, C. F. Macrae, P. McCabe, J. Pearson, and R. Taylor, New software for searching the Cambridge Structural Database and visualizing crystal structures, *Acta. Crystallogr. B. Struct. Sci.* **58**, 389 (2002).
- [82] D. Li, X.-M. Zhao, H.-X. Zhao, L.-S. Long, and L.-S. Zheng, Coexistence of Magnetic-Optic-Electric Triple Switching and Thermal Energy Storage in a Multifunctional Plastic Crystal of Trimethylchloromethyl Ammonium Tetrachloroferrate(III), *Inorg. Chem.* **58**, 655 (2019).
- [83] L. A. K. Staveley, Phase transitions in plastic crystals, *Annu. Rev. Phys. Chem.* **13**, 351 (1962).
- [84] P.-F. Li, Y.-Y. Tang, W.-Q. Liao, H.-Y. Ye, Y. Zhang, D.-W. Fu, Y.-M. You, and R.-G. Xiong, A semiconducting molecular ferroelectric with a bandgap much lower than that of BiFeO₃, *NPG Asia Mater.* **9**, e342 (2017).
- [85] Y. Bai, H. Jantunen, and J. Juuti, Energy Harvesting Research: The Road from Single Source to Multisource, *Adv. Mater.* **30**, 1707271 (2018).
- [86] H.-Y. Liu, H.-Y. Zhang, X.-G. Chen, and R.-G. Xiong, Molecular Design Principles for Ferroelectrics: Ferroelectrochemistry, *J. Am. Chem. Soc.* **142**, 15205 (2020).
- [87] J.-H. Lin, J.-R. Lou, L.-K. Ye, B.-L. Hu, P.-C. Zhuge, D.-W. Fu, C.-Y. Su, and Y. Zhang, Halogen Engineering To Realize Regulable Multipolar Axes, Nonlinear Optical Response, and Piezoelectricity in Plastic Ferroelectrics, *Inorg. Chem.* **62**, 2870 (2023).
- [88] G. Iñiguez, F. Battiston, and M. Karsai, Bridging the gap between graphs and networks, *Commun. Phys.* **3**, 88 (2020).